Distinctive fatigue properties of additively-formed CoCrFeNiTiMo multi-principal element alloy: excellent fatigue crack growth resistance against ordinally high cycle fatigue strength

Hideaki Nishikawa[1], Yoshiyuki Furuya[1], Houichi Kitano[1], Yoshiharu Kanegae[2], Kinya Aota[2], Kosuke Kuwabara[2]

Affiliation

[1]Research Center for Structural Materials (RCSM), National Institute of Materials Science (NIMS), 1-2-1 Sengen, Tsukuba 305-0047, Japan

[2]Global Research and Innovative Technology center (GRIT), Proterial, Ltd. 5200 Mikajiri, Kumagaya, Saitama, 360-8577, Japan

Corresponding author:

Hideaki Nishikawa

e-mail: NISHIKAWA.Hideaki@nims.go.jp

Abstract

In this study, the fatigue characteristics of additively-formed multi-principal element alloy (MPEA) of $Co_{1.5}CrFeNi_{1.5}Ti_{0.5}Mo_{0.1}$ (CoCrFeNiTiMo alloy) were systematically compared with conventional hot-rolled and additively-formed Alloy 718 nickel-based super alloy, which have comparable mechanical properties. Evaluated fatigue properties were the low- to high-cycle fatigue strengths of plane and notched specimens, and long / short fatigue crack growth (FCG) resistance. The results showed the fatigue strength of CoCrFeNiTiMo alloy to be comparable to that of Alloy 718 for smooth specimens, while the fatigue strength of notched specimens was 50 % higher. Superior notch fatigue strength can be quantitatively explained in terms of outstanding long fatigue crack growth resistance. Regardless of load ratio, CoCrFeNiTiMo exhibits superior FCG resistance that greatly surpasses that of conventional Fe and Ni alloys. In contrast, the short FCG resistance of CoCrFeNiTiMo was comparable to that of Alloy 718, which corresponds to the fatigue strength level of a smooth specimen. Investigation of fatigue fracture surface and microscopic slip deformation morphology around the fatigue crack indicates that CoCrFeNiTiMo alloy exhibits more planar slip deformation than Alloy 718. Slip constraint stimulated by slip planarity appears to have an important role in short and long FCG resistance when cracks cross grain boundaries.

Keywords: Multi-principal element alloy, Additive manufacturing, Fatigue, Short fatigue crack, Slip planarity

1. Introduction

The alloying concept of high entropy alloys (HEAs) was first proposed by Cantor et al. [1] and Yeh et al. [2] in 2004. HEAs are usually defined as solid-solution alloys without intermetallic compounds, consisting of five or more elements with concentrations of between 5 and 35 at.%. Multi-principal element alloys (MPEAs) were proposed by Senkov et al. [3] to broaden the alloy variation of HEAs, allowing the presence of secondary phases such as intermetallic precipitations in the solid solution matrix. In this study, these alloys are hereinafter collectively referred to as MPEAs. The outstanding mechanical properties of MPEAs have recently been reported [4,5]. One of our authors has developed a precipitation-hardened CoCrFeNiTi-based MPEA, $Co_{1.5}CrFeNi_{1.5}Ti_{0.5}Mo_{0.1}$, which has excellent mechanical properties and corrosion resistance [6–9]. This alloy was developed based on the HEAs proposed by Chou et al., [10,11] and is strengthened by precipitation hardening that is managed by solidification control during the additive manufacturing process and post-heat treatments. It exhibits outstanding mechanical properties, with a tensile strength that exceeds 1,500 MPa. However, to be able to use this alloy as a structural material, it is necessary to understand its fatigue property. This alloy is hereinafter referred to as CoCrFeNiTiMo alloy.

A range of fatigue properties of MPEAs have been reported, which extend from normal to excellent. For example, Ritchie et al. reported the outstanding fatigue crack growth (FCG) resistance of a CrCoNi Medium entropy alloy under cryogenic conditions [12]. More recently, Li et al. reviewed and re-organized the published fatigue data for MPEAs [13]. They report the ratio between high cycle fatigue strength and tensile strength of MPEAs to be distributed from 0.3 - 0.5, which is comparable to the

usual proportional ratio of fatigue strength of conventional steels, titanium and aluminium alloys [14–16]. In contrast, the FCG data showed ΔK – da/dN in MPEAs to be widely distributed but included excellent FCG resistance [17].

One of the possible unique features related to the fatigue performance of MPEAs is variable stacking fault energy (SFE) which affects deformation mechanisms such as slip planarity and twinning [18]. Several reports have focused on this problem, since MPEAs potentially have a wide range of SFEs [19]. This type of deformation mechanism is likely to affect fatigue behaviour, since microscopic fatigue crack initiation and growth mechanisms are governed by slip deformation [20,21]. For example, Koyama et al. report that planar slip leads to intermittent crack initiation ahead of the fatigue crack tip [22]. Although it has long been observed that slip planarity influences fatigue behaviour [22–24], systematic investigation is still lacking. For example, the effect of slip planarity on fatigue properties, such as high cycle fatigue property and FCG property, have usually been discussed as individual cases. Comparative studies which use materials that have similar mechanical strength level are rare, although fatigue property appears to be closely related to tensile and yielding strengths. In addition, the short fatigue crack growth behaviour of MPEAs, which is a fundamental damage process in fatigue failure [25] has rarely been reported.

In our experiments, the tensile strength level of CoCrFeNiTiMo alloy was comparable to that of Ni-based superalloys such as Alloy 718; however, CoCrFeNiTiMo alloy appears to exhibit more planar slip due to lower SFE caused by its higher Co content [26]. In this study, to reveal the individual features of the fatigue property of MPEAs and their metallurgical background, a systematic fatigue evaluation

of CoCrFeNiTiMo alloy and Alloy 718 was conducted from the perspective of the effect of slip planarity on fatigue properties.

2. Materials

The materials used in this study were CoCrFeNiTiMo alloy and Ni-based Alloy 718. CoCrFeNiTiMo alloy has a face-centred-cubic (γ) matrix and includes strengthening nanoprecipitates such as ordered $L1_2$ crystal structure (γ′) [7,9]. For Alloy 718, commercial hot-rolled plate and additively-formed samples were prepared for comparison. Table 1 shows the nominal alloy compositions of these alloys. Additively-formed samples were fabricated using the selective laser melting (SLM) feature of an EOS M290 3D printer. Table 2 shows the SLM building conditions. The fatigue specimen samples were fabricated as rectangular parallelepipeds. All the samples were heat-treated before machining as fatigue specimens. CoCrFeNiTiMo alloy samples were solution heat-treated at 1120 ˚C for 1 hour followed by gas quenching in nitrogen. The products were subjected to aging heat treatment at 620 ˚C for 8 hours in an atmospheric furnace. For hot-rolled and additively-formed Alloy 718, subsequent solution treatment was performed at 980 ˚C for 1 hour followed by cooling in air, then double aging at 720 ˚C for 8 hours, and cooling to 620 ˚C at 50 ˚C/hour. The sample was then held for 8 hours at 620 ˚C in a vacuum furnace.

Figures 1 and 2 show microstructure images and inverse pole figure (IPF) maps of electron backscatter diffraction (EBSD) analysis of used alloys. CoCrFeNiTiMo alloy and hot-rolled Alloy 718 has equiaxed grains. The crystallographic texture, which affects fatigue property [27,28], was not observed in these materials. Average grain size

as evaluated using EBSD data based on fractions of rolled Alloy 718, additively-formed Alloy 718 and CoCrFeNiTiMo alloy, the were 32, 57 and 56 μm respectively.

Table 1. Nominal alloy composition (wt.%)

Material	Co	Ni	Fe	Cr	Nb	Mo	Al	Ti	Ta	Si	Mn	P	S	C	B
Hot-rolled Alloy 718	-	Bal.	18.4	18.3	5.14	3.00	0.46	0.98	-	0.11	0.09	0.007	0.0002	0.030	0.001
Alloy 718 powder	-	Bal.	20.1	17.0	5.41	3.10	0.50	0.94	-	0.01	<0.01	<0.001	0.0002	0.058	-
CoCrFeNiTiMo powder	Bal.	23.5	13.9	17.5	-	3.88	-	3.64	3.08	-	-	-	-	-	0.010

Table 2. Building conditions of SLM

Material	Equipment	Building conditions
Alloy 718	EOS M290	Layer thickness: 0.04 mm, Hatch spacing: 0.11 mm, Pre-heat temperature: 80 °C, Lasor power: 285 W, Scanning speed: 980 mm/s
CoCrFeNiTiMo	EOS M290	Layer thickness: 0.04 mm, Hatch spacing: 0.09 mm, Pre-heat temperature: 80 °C, Laser power: 300 W, Scanning speed: 1300 mm/s

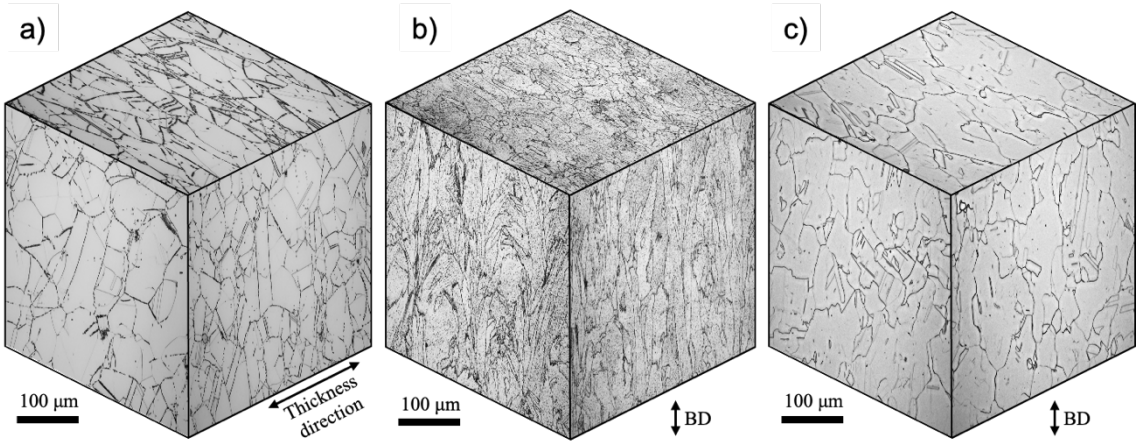

Figure 1. Microstructure images of a) hot-rolled Alloy 718, b) additively-formed Alloy 718 and c) CoCrFeNiTiMo alloy

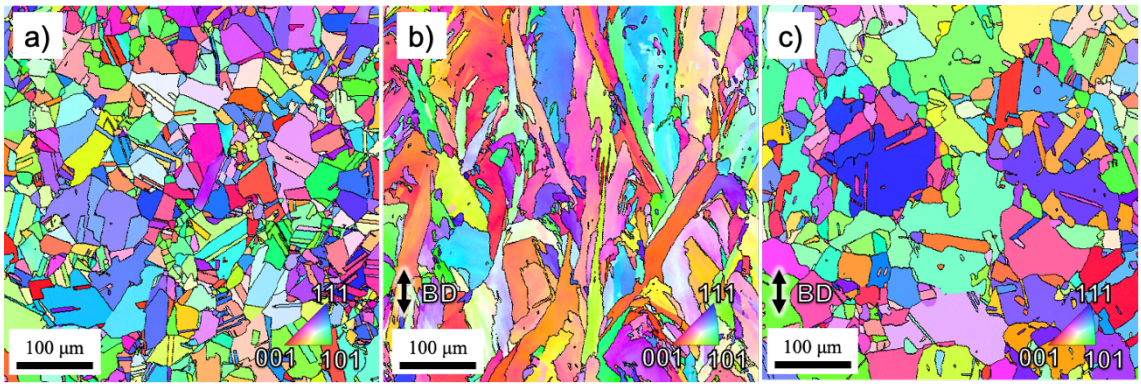

Figure 2. IPF map images for a) hot-rolled Alloy 718, b) additively-formed Alloy 718 and c) CoCrFeNiTiMo alloy

3. Testing procedure

In this study, compact tension (CT) specimens were subjected to axial loading fatigue testing and crack growth testing. The axial-loaded fatigue tests were conducted using a servo hydraulic-type fatigue testing machine under load-controlled conditions with a stress ratio of –1. As shown in Fig. 3, three types of specimens were used in axial-loaded fatigue tests. The specimen surfaces in Fig. 3 a) were polished with emery paper from grades 240 - 600 in the longitudinal direction. The hatched area of the specimen in Fig. 3 b) was chemically etched after mirror polishing to remove the work-hardened layer and to reveal its microstructure for *in situ* observation. The stress concentration factor of the notch root of Fig. 3 c) was about 4.9. Axial strain-controlled incremental step tests [29] were also conducted to evaluate cyclic yielding strength using the specimen shown in Fig. 3 a). The gage length was 3 mm and strain rate was 5 x 10^{-3}/s in the strain-controlled fatigue test. The other testing conditions were the same as in our previous study [30].

Long fatigue crack growth tests were conducted using the back face strain gage method by using compact tension (CT) specimens according to ASTM E647 [31]. The CT specimen size used in this study was W = 48 mm and 8 mm thickness. The accuracy of crack length measurements was confirmed and corrected by checking the fatigue fracture surface after the crack growth test. Short fatigue crack initiation and growth behaviour was observed with the specimen type shown in Fig 3 b) using an in-house-designed automatic microscope observation system [32]. For this observation, panoramic images of specimen surfaces were automatically captured at regular intervals of fatigue cycles during fatigue testing to detect microscopic initial fatigue cracks.

The loading directions in the axial loading fatigue test were the same as the building direction (BD) of additively-formed specimens. The CT MPEA specimens were prepared with three BDs: the transverse direction (TD) and 45-degree diagonal directions (DD) to confirm FCG anisotropy.

After the fatigue tests, microscopic details were partly observed with EBSD and Electron Channelling Contrast (ECC) by using JEOL JSM-7900F. ECC observations were conducted by using a backscattered-electron detector operating at accelerating voltage of 20 kV and working distance of 4.0 mm.

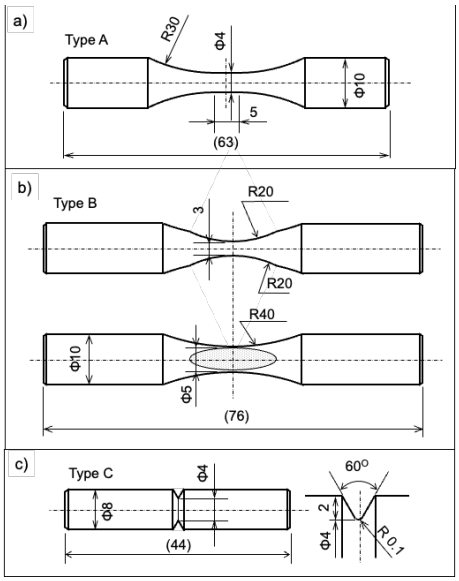

Figure 3. Specimen configurations of a) emery-polished specimen, b) chemically-etched specimen for *in situ* observation and c) notched specimen.

4. Results

4.1 Monotonic and cyclic yielding strength

Table 3 shows the mechanical properties and Figure 4 shows the monotonic and cyclic stress strain relations. As shown in the Table 3, the tensile strength and Young's modulus of CoCrFeNiTiMo alloy were comparable to those for Alloy 718, and the elastic and plastic anisotropy of CoCrFeNiTiMo alloy was small. As illustrated on the Fig. 4 a), stress-strain curves of monotonic tensile tests were made from the data of strain gage, gage length and cross head displacement for comparison. As shown in this figure, CoCrFeNiTiMo alloy exhibit large work hardening compared to Alloy 718. Large work hardening is one of the feature of the material which appears planar slip deformation [33]. Although the monotonic 0.2 % proof strength of CoCrFeNiTiMo alloy was slightly lower than that of Alloy 718, the cyclic yielding strength, as shown in Fig. 4 b), was comparable to that of Alloy 718, since Alloy 718 exhibited cyclic

softening during strain-controlled fatigue testing. High-cycle fatigue strength is usually related to tensile strength or cyclic yielding strength [14–16]. Hence, future comparative studies will be able to evaluate the fatigue features of MPEAs, such as the effect of slip planarity, separately from their mechanical properties.

Table 3. Mechanical properties

Material	Loading direction	0.2 % proof strength	Ultimate tensile strength	Elongation	Reduction of area	*Young's Modulus
		MPa	MPa	%	%	GPa
Hot-rolled Alloy 718	Rolling direction	1146	1367	27	41	210
Additively-formed Alloy 718	Building direction	1179	1350	24	38	200
CoCrFeNiTiMo alloy	Building direction	901	1359	39	44	222
	Transverse direction	914	1382	39	45	228
	Diagonal direction	918	1384	37	44	225

*Evaluated from stress-strain curves of tensile tests

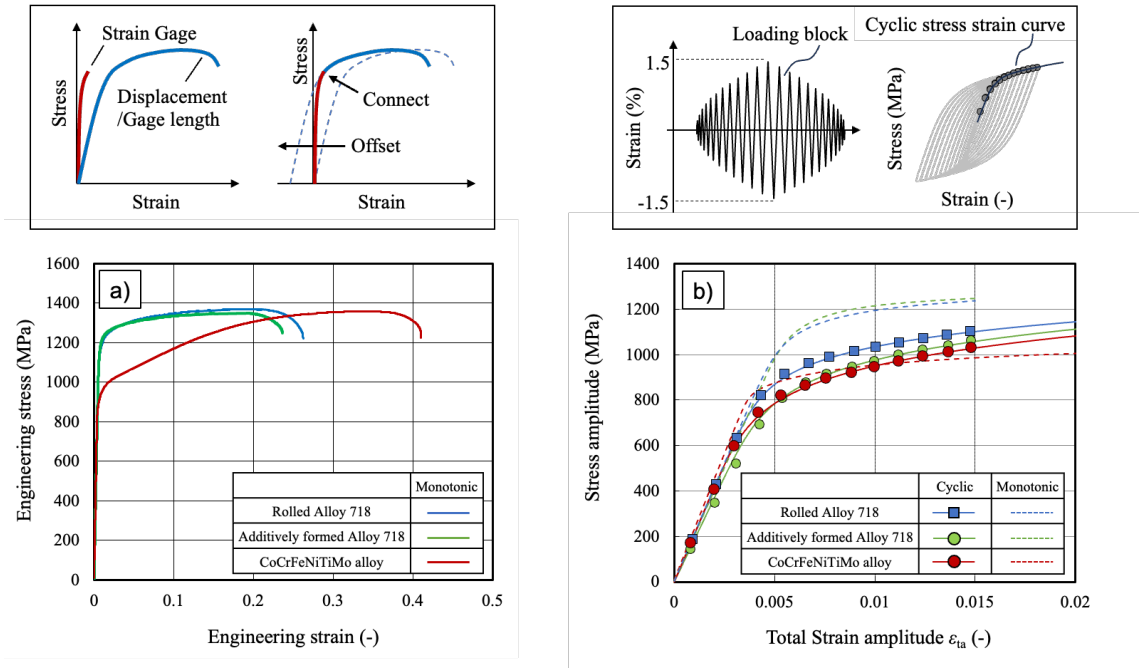

Figure 4. Stress strain relationship for a) monotonic and b) cyclic loading

4.2 Fatigue strength and long fatigue crack growth property

Figure 5 is an S-N diagram that includes the three types of specimens shown in Figure 3. The S-N curve of rolled Alloy 718 and additively-formed Alloy 718 were almost the same regardless of specimen type. Fatigue data on Alloy 718 for smooth specimens were partly reported in our previous work [27]. The fatigue strength of CoCrFeNiTiMo alloy for smooth type A and B specimens in Fig. 3 were comparable to that of Alloy 718, while that of the type C notched specimen was 50 % higher than that of Alloy 718. It is worthy of note that the fatigue strength of etched smooth specimens was lower than that of polished smooth specimens because the work-hardening layer had been removed by buff polishing and chemical etching.

Figure 6 shows the long fatigue crack growth properties of the three materials. The *K* decreasing and increasing FCG tests were conducted under a load ratio of R = 0.1. More data for higher load ratios were obtained in the *K* decreasing test. As shown in this figure, the CoCrFeNiTiMo alloy exhibits far better crack growth resistance than Alloy 718, regardless of load ratio. ΔK_{th} was higher and the fatigue crack growth rate (FCGR) was slower than with Alloy 718. FCGR anisotropy was not observed in this alloy. The FCGR of rolled and additively-formed Alloy 718 was comparable. The fatigue strength gap with the notched specimen shown in Fig. 5 therefore corresponds to the FCGR properties of the CT specimens.

Figure 7 represents the relationship between ΔK_{th}, stress ratio and maximum stress intensity of K_{max}. The data range for a hundred Fe and Ni alloys as organized by Liaw et al. [34] is also represented in Fig. 7a). As shown in this figure, the ΔK_{th} value of CoCrFeNiTiMo alloy was much higher than that of any other Fe and Ni alloys. Figure 7 b) shows K_{max} versus ΔK_{th}. Vasudévan et al. proposed the existence of two regions, the K_{max}-constant region and the ΔK_{th}-constant region, in long crack growth thresholds [35–37]. As shown in Fig. 7 b), CoCrFeNiTiMo is superior to Alloy 718 in each region. In the later high-R region, ΔK_{th} appears to be the same as $\Delta K_{eff\,th}$. In other words, the reason for the excellent long crack growth property of CoCrFeNiTiMo alloy cannot be accounted for by the crack closure effect [38,39]. Work hardening difference in monotonic tensile test possibly changes crack closure through the change of monotonic plastic zone size while this is not enough to explain the FCGR resistance of CoCrFeNiTiMo alloy.

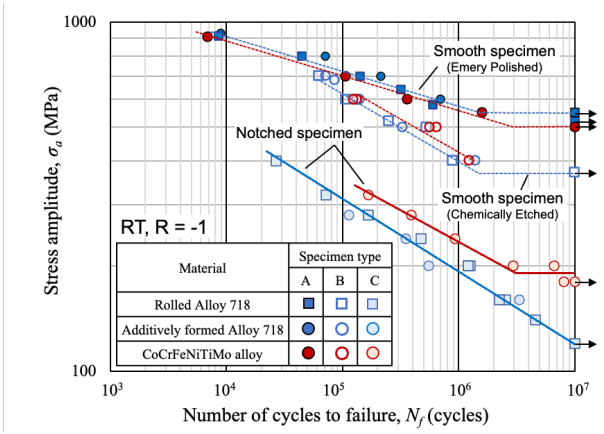

Figure 5. S-N diagram

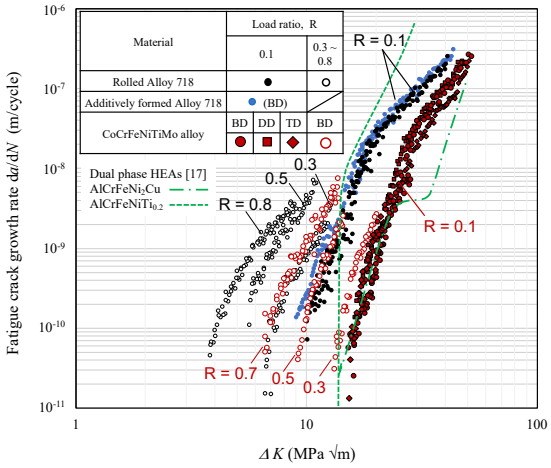

Figure 6. Long fatigue crack growth properties for variable load ratios measured using CT specimens. MPEAs under conditions of R = 0.1 were tested using three loading directions that correspond to the BD, DD and TD in the additive process specimens.

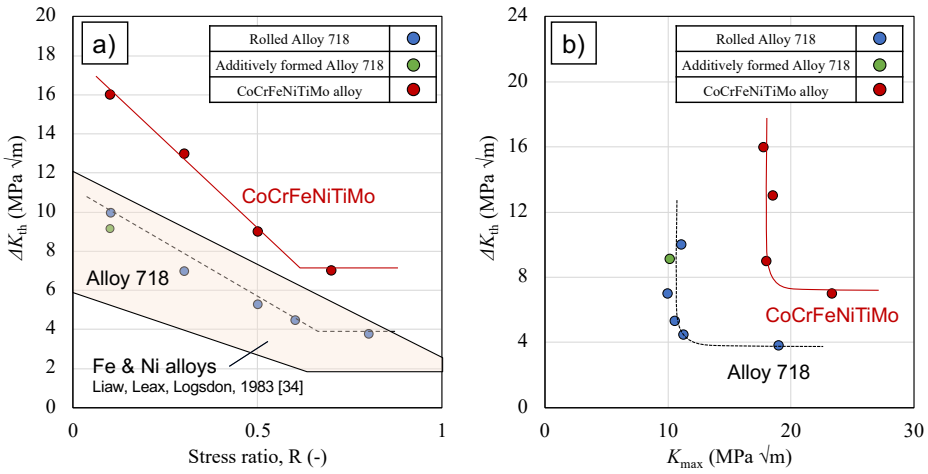

Figure 7. Threshold stress intensity factor range, ΔK_{th} versus a) stress ratio and b) maximum stress intensity factor, K_{max}

4.3 Short fatigue crack growth behaviour

To understand the pattern of the S-N curve and long crack growth behaviour, the surface short fatigue crack initiation and growth behaviours of Alloy 718 and CoCrFeNiTiMo alloy were investigated, since the fatigue life of smooth specimens is usually dictated by small fatigue crack growth life.

Figures 8 and 9 show examples of microscopic crack initiation behaviours for rolled Alloy 718 and CoCrFeNiTiMo alloy. White arrows indicate the crack tip positions of each image. In this study, all observed fatigue cracks, including in additively-formed specimens, were initiated from the microstructure, with no defects being observed at the crack initiation area. Fatigue cracks appeared to form along slip planes in the early stage of the fatigue cycle. During the fatigue cycle, fretting debris was generated from the cracks.

Figure 10 shows growth curves of SFCs (small fatigue cracks) at two different stress amplitude levels. Fatigue cracks were first detected at about 5 - 38 % of total fatigue life. Hence, the major proportion of the total fatigue life was accounted for by the crack growth process. A greater number of fatigue cracks were initiated in CoCrFeNiTiMo than in Alloy 718, so examples of sub crack growth behaviour are also plotted in Fig. 10 a). SFC growth rates are illustrated in Figure 11. The long crack data shown in Fig. 6 is superimposed on this figure. Most SFC growth rates of the three materials were comparable, whereas sub cracks in CoCrFeNiTiMo alloy grew more slowly than the others. All SFC growth rates were faster than that for long cracks. The rolled Alloy 718 data shows that SFC growth rates gradually approached those of long cracks at high load ratios as ΔK increased. In contrast, the data for SFC growth rates in CoCrFeNiTiMo were entirely different from those of long crack data.

The ΔK - da/dN curve under high load ratios is usually the same as the ΔK_{eff} - da/dN curve; hence, the changes in SFC growth rates in Alloy 718 may have been chiefly related to the crack closure effect. In contrast, the difference between the short and long crack growth rates in CoCrFeNiTiMo appears too wide to be explained solely by the crack closure effect. One other possible reason for the fast SFC growth rates is the inhomogeneous chemical composition around the crack initiation area. This prompted use to examine the distribution of the chemical composition around the crack initiation area using energy-dispersive X-ray spectroscopy (EDS). As shown in Fig. 12, however, no uneven composition was observed around the crack initiation area. It is necessary to consider some other mechanism, such as the role of slip planarity, to explain these experimental results.

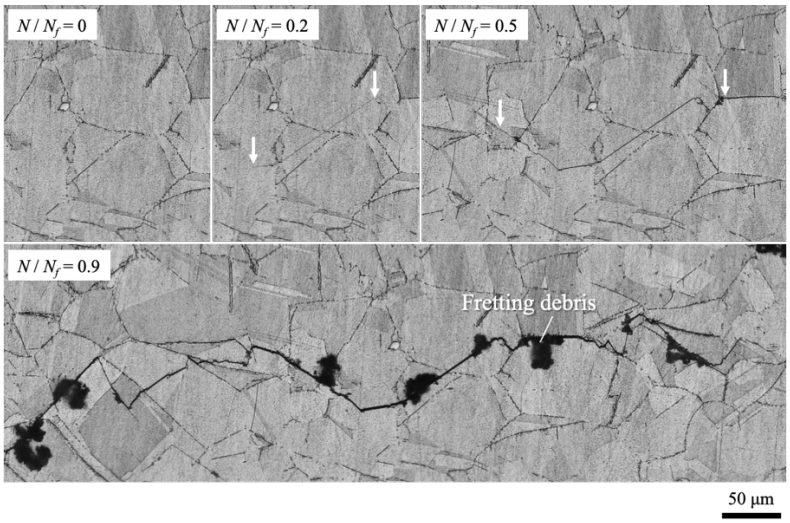

Figure 8. Small fatigue crack initiation and growth behaviour of hot-rolled Alloy 718. σ_a = 600 MPa, N_f = 1.3 x 10^5 cycles.

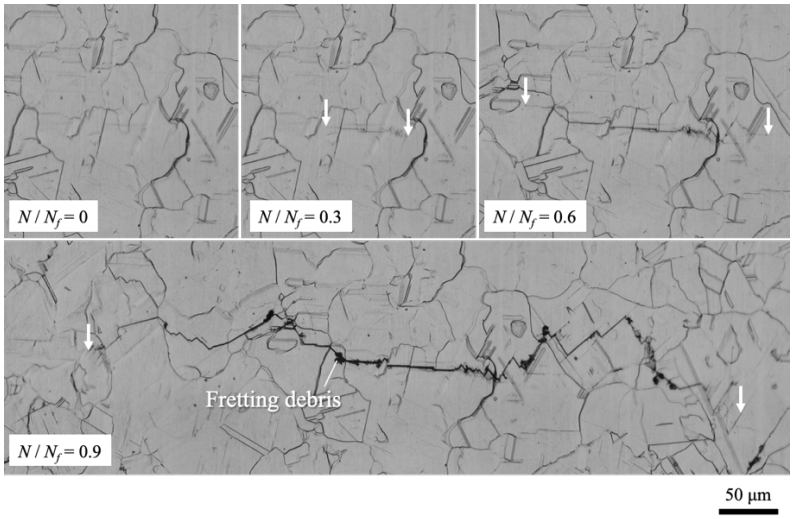

Figure 9. Small fatigue crack initiation and growth behaviour of AM CoCrFeNiTiMo alloy. σ_a = 600 MPa, N_f = 1.3 x 10^5 cycles.

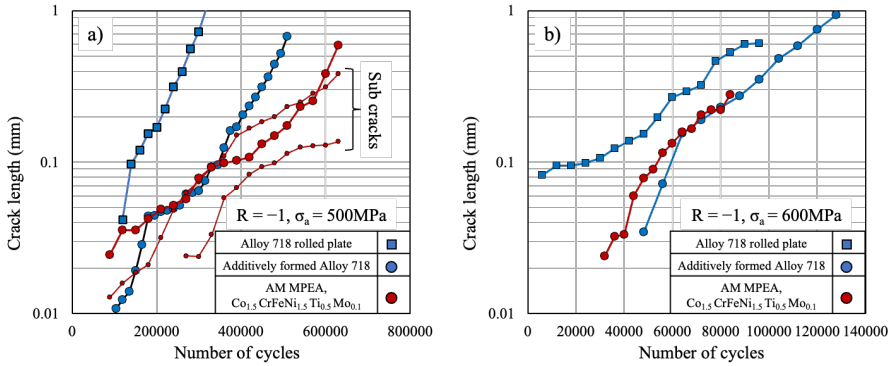

Figure 10. Small fatigue crack growth curve tested under stress amplitude of a) 500 MPa and b) 600 MPa.

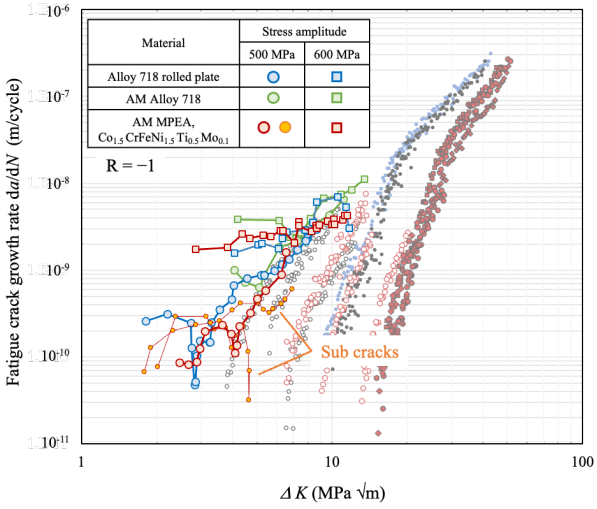

Figure 11. Growth rate of short fatigue cracks superimposed on the long crack data shown in Fig. 6.

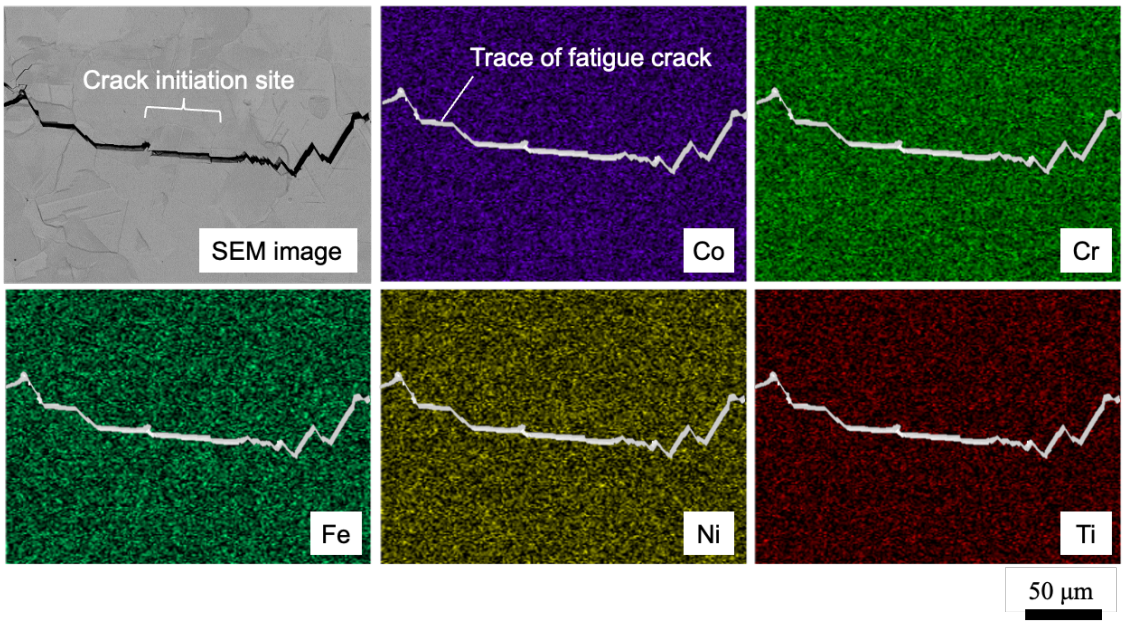

Figure 12. Energy-dispersive X-ray spectroscopy (EDS) analysis around the fatigue crack initiation area of Fig. 9.

4.4 Fracture surface morphology

The fatigue fracture surface morphologies of Alloy 718 and CoCrFeNiTiMo alloy are represented in Figures 13 and 14 respectively. Figures a) and b) show observations on CT specimens as long cracks, and Figs c) show observations on smooth specimens as short cracks. All images were captured where the FCGR area was close to 1 x 10^{-9} m/cycle. The fracture surface of CoCrFeNiTiMo alloy tends to show more large blocky facets than Alloy 718. Here, if the FCGR curve changes due to the crack closure effect, the fatigue fracture surface morphology should be the same if the FCGR is the same. As shown in Fig. 13 a) to c) of Alloy 718, there were no obvious differences except for fretting debris appearing on the smooth specimen. We therefore concluded the FCGR curve of Alloy 718 for this region to vary in relation to the crack closure effect. In contrast, the fatigue fracture surface of CoCrFeNiTiMo alloy tended to vary with the

testing conditions even though the FCGR values were the same. For example, as shown in Fig. 14, larger facets appear to be more noticeable, especially under high road ratios. It appears necessary to take into account factors other than crack closure to be able to elucidate the FCG behaviour of CoCrFeNiTiMo alloy.

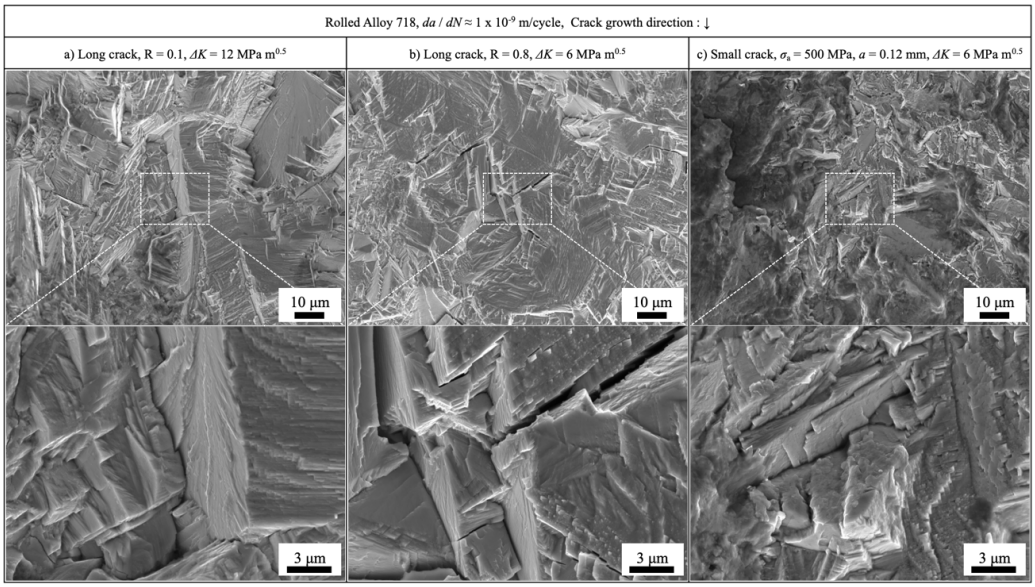

Figure 13. Fatigue fracture surface morphologies for rolled Alloy 718 observed in long cracks in the CT specimens and small cracks in the smooth specimens for the same FCGR area of 1 x 10^{-9} m/cycle.

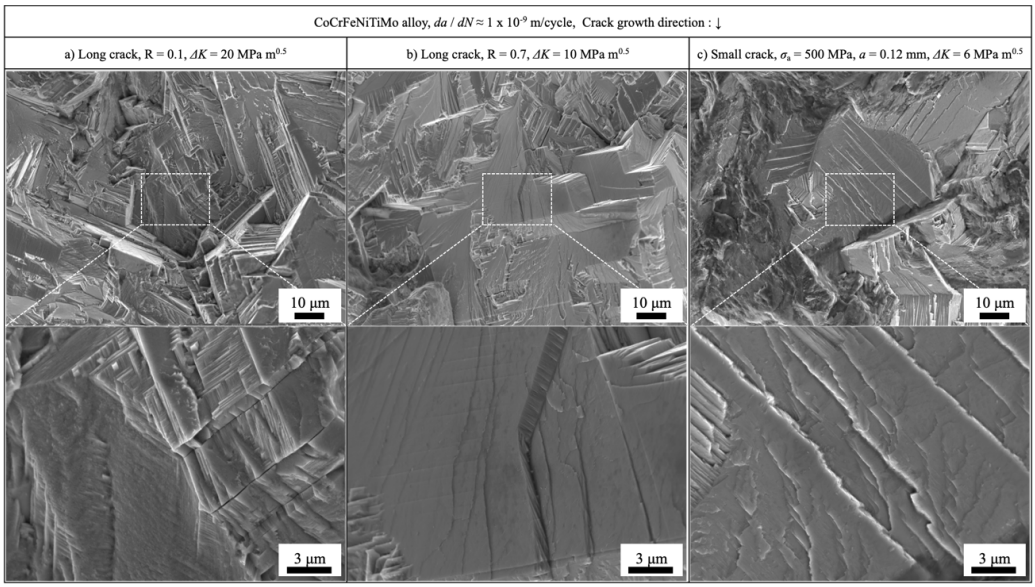

Figure 14. Fatigue fracture surface morphologies in AM CoCrFeNiTiMo alloy observed in long cracks in the CT specimens and small cracks in the smooth specimens for the same FCGR area of 1 x 10^{-9} m/cycle.

4.5 Microscopic deformation morphologies of short fatigue cracks

To clarify microscopic deformation behaviours during FCG, we conducted ECC observations of incremental step fatigue test and cross-sectional SEM / EBSD analysis of short fatigue cracks.

Figure 15 shows ECC images observed after incremental step fatigue tests, which were shown in figure 4, of Alloy 718 and CoCrFeNiTiMo alloy. These images were observed at the cross-section 1.5 mm away from the fracture surface. As shown in these images, slip deformations related to the fatigue tests were revealed with ECC. The yellow dotted lines in the figures indicate the trace of typical direction of slip lines. As shown in Fig. 15 a), there were two different slip lines which intersected each other. Hence, it is considered that primary and secondary slip systems were activated in Alloy

718. In contrast, CoCrFeNiTiMo alloy usually shows the grains which has slip traces with single direction as shown in Fig. 15 b). It is considered that the secondary slip system in CoCrFeNiTiMo alloy was less likely to be activated than that in Alloy 718 possibly due to the difference of slip planarity.

Figures 16 and 17 respectively show cross-sectional observations of short fatigue cracks in rolled Alloy 718 and CoCrFeNiTiMo alloy. The observation samples were prepared from sub cracks on the broken fatigue specimens. The cutting positions of the samples were close to the centre of the surface crack length. The sample surfaces were finished with a broad ion beam cross section polisher. The fatigue crack images were captured using backscattered electron (BSE) imaging. Kernel average misorientation (KAM) and grain orientation spread (GOS) maps were analysed with EBSD to reveal slip deformation behaviour around the short fatigue cracks. The KAM value is normally related to local deformation and the GOS value is related to the total deformation of the grain. Koyama et al. reported that GOS value was proportional to the dislocation density [40].

As shown in Fig. 16 c) and Fig. 17 c), the area of high KAM value for Alloy 718 was more broadly distributed than in the CoCrFeNiTiMo alloy. In addition, the GOS values around the cracks in Alloy 718 were relatively higher than those for the CoCrFeNiTiMo alloy. As shown in Fig. 17 c), there were few visible deformations around the fatigue cracks in the CoCrFeNiTiMo alloy. It note that, part of the crack in Fig. 17 propagated close to the boundaries, while these boundaries were consistent with recrystallization twin boundary of FCC according to EBSD analysis. Fatigue crack of FCC material usually formed in the slip band along twin boundary because which is

{111} slip plane as well [41,42]. Therefore, fatigue crack in Fig. 17 possibly propagated with slip deformation.

Figure 18 shows the microscopic morphology of the crack tip on the specimen surface of CoCrFeNiTiMo alloy. As shown in this image, planar slip bands were observed and fatigue cracks appear to have propagated along the slip plane.

These results indicate that slip deformation during SFCG of the CoCrFeNiTiMo alloy appears to be more concentrated near the crack than seen in Alloy 718, possibly due to the difference in slip planarity. This different planar slip deformation of CoCrFeNiTiMo alloy is also likely to affect long fatigue crack growth.

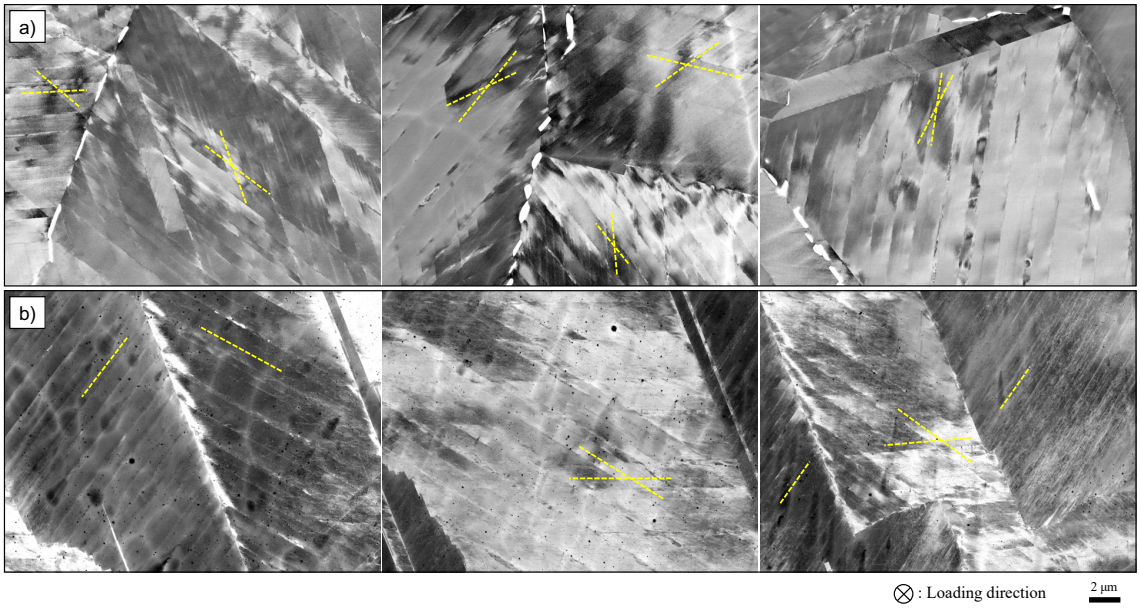

Figure 15. ECC images observed after incremental step fatigue tests for a) rolled Alloy 718 and b) CoCrFeNiTiMo alloy

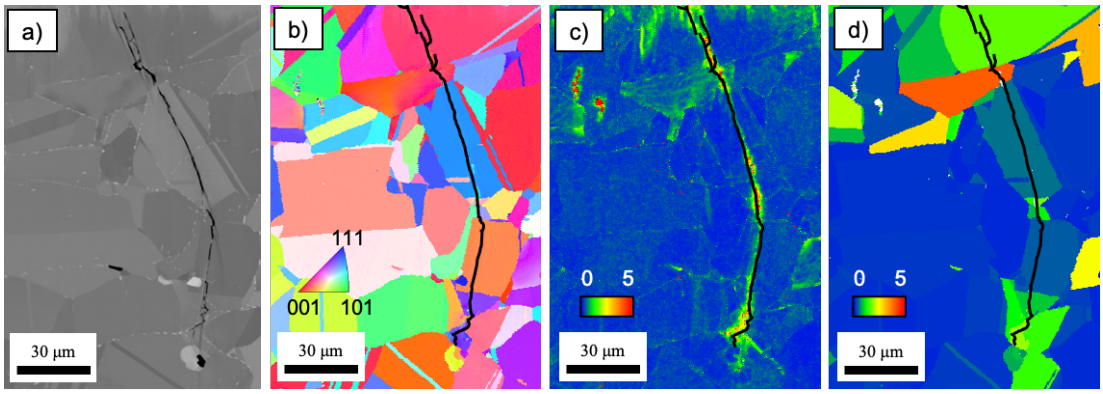

Figure 16. Cross-sectional observation of short fatigue crack for rolled Alloy 718 of a) BSE image, b) IPF map, c) KAM map, and d) GOS map. σ_a = 600 MPa, N_f= 1.3 x 10^5. The solid line indicates the trace of the fatigue crack. The crack length from the surface was about 0.19 mm.

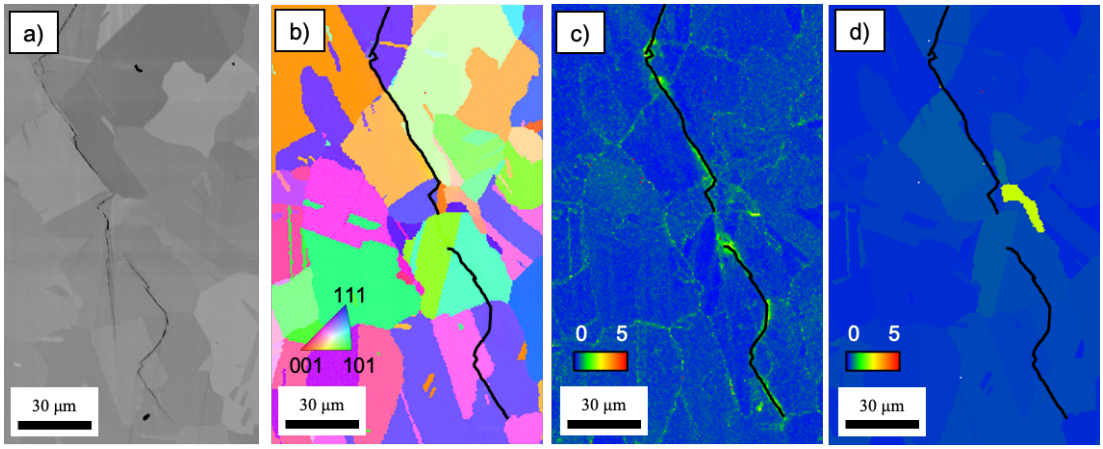

Figure 17. Cross-sectional observations of a short fatigue crack in CoCrFeNiTiMo alloy. a) BSE image, b) IPF map, c) KAM map, d) GOS map. σ_a = 500 MPa, N_f= 6.5 x 10^5. The solid line indicates the trace of the fatigue crack. The crack was about 0.26 mm long and started from the surface.

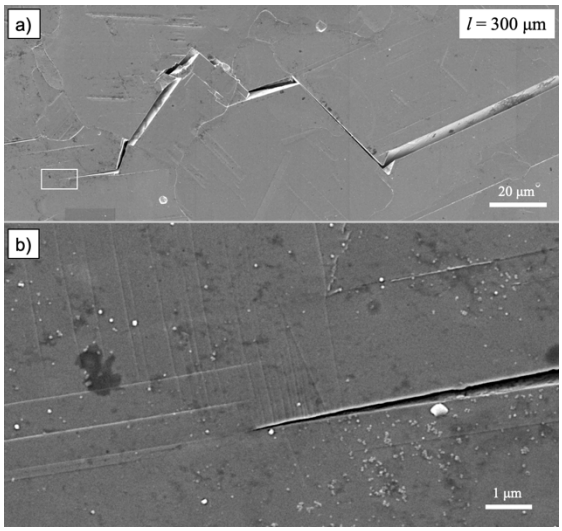

Figure 18. SEM image at the short fatigue crack tip of the specimen surface for CoCrFeNiTiMo alloy. b) shows an enlargement of the boxed area in a). σ_a = 600 MPa, N_f = 1.3 x 10^5 cycles.

5. Discussion

5. 1 Fatigue strength level of CoCrFeNiTiMo alloy

The fatigue data for CoCrFeNiTiMo alloy were first compared to empirical data and equations. The fatigue limit σ_w of smooth specimens is usually proportional to material tensile strength σ_B. Hence, it is not surprising that Alloy 718 and CoCrFeNiTiMo alloy, which have similar tensile strength, showed comparable fatigue strength levels, as illustrated the in S-N diagram in Figure 5. In addition, normal fatigue strength ratios of σ_w / σ_B under R = –1 are 0.53 for martensitic steels and 0.39 for austenitic stainless steels [14]. These proportional coefficients of titanium [15] and aluminium alloys [16] are also 0.53 and 0.39 respectively. As seen in Fig. 5, the fatigue strength ratios of Alloy 718 and CoCrFeNiTiMo alloy were about 0.42 and 0.39, i.e., not inferior to

conventional steels. In contrast, as shown in Fig. 5, CoCrFeNiTiMo exhibits far better notch fatigue strength than Alloy 718, although the notch sensitivity of fatigue strength is usually related to tensile strength level [43].

This superior notch fatigue strength was related to the very good long fatigue crack growth resistance shown in Figs. 6 and 7. The stress concentration factor of the notch root, $K_t = 4.9$, is large enough to regard the notch as a crack. Adopting a fracture mechanics approach, empirical equations to estimate fatigue strength for sharp notch [44,45] are expressed as

$$a_0 = \frac{1}{\pi}\left(\frac{\Delta K_{th}}{\sigma_w}\right)^2 \quad (1),$$

and

$$K_f = \frac{\sigma_w}{\sigma_{wn}} = \sqrt{1 + \frac{a}{a_0}}, \quad (2),$$

where σ_w is the fatigue strength of a smooth specimen, σ_{wn} is the fatigue strength of a notched specimen, and a is notch size. According to these equations, the notch fatigue strength of rolled Alloy 718 and CoCrFeNiTiMo alloy calculated with ΔK_{th} of $R = 0.1$ were 123 and 188 MPa respectively, which corresponds to the tensile part of the stress amplitude when R = –1. These calculated values were very close to the experimental results. Note that notch fatigue strengths of high strength steels were usually below 100 MPa, because ΔK_{th} decreases as tensile strength increases [46]. Hence the excellent notch fatigue strength of CoCrFeNiTiMo alloy is to be expected in the context of its outstanding long fatigue crack growth property. In other words, the level of long fatigue crack growth resistance was higher than anticipated.

As shown in Fig. 7, ΔK_{th} of CoCrFeNiTiMo was clearly higher than the data distribution range of Fe and Ni alloys which includes more than a hundred items of ΔK_{th}

data organized by Liaw et al. [34]. They also organized published FCG data of HEAs which have ΔK_{th} values distributed from 2 - 17 MPa $m^{0.5}$ [13]. According to their evaluation, dual phase FCC + BCC HEAs [17] showed the highest level of FCG resistance, as seen superimposed on Figure 6. As can also be seen in Fig. 6, CoCrFeNiTiMo alloy exhibited FCG resistance comparable to these dual phase HEAs. In other words, CoCrFeNiTiMo alloy has the highest level of FCG resistance ever officially published. Note that FCGR is normally related to Young's modulus [47]. The Young's modulus of CoCrFeNiTiMo was 222 GPa, comparable to that of Alloy 718.

5. 2 Effect of slip planarity on long and short fatigue crack growth property

In contrast to that of long cracks, short fatigue crack growth resistance of CoCrFeNiTiMo was comparable to that of Alloy 718, as shown in Figs. 10 and 11. It is possible that one critical difference between these two alloys is slip planarity. Slip planarity possibly changes the crack tip deformation mode and leads to the formation of flat facets on the fracture surface. To understand the above complex difference between long and short FCG behaviour, the effects of slip planarity are discussed here.

Slip planarity is related to stacking fault energy (SFE). The slip system, grain size, and precipitation hardening also affect slip planarity [48]. Slip deformation of CoCrFeNiTiMo appears to be more planar than that of Alloy 718 because the SFE of CoCrFeNiTiMo, which has a higher Co content, appears to be lower than that of Alloy 718; the SFE value at room temperature, calculated using *JMatPro*® commercial software, was 47 mJ/m^2 for CoCrFeNiTiMo and 202 mJ/m^2 for Alloy 718. In this software, SFE is calculated based on Gibbs free energy difference between FCC and HCP structures by using the CALculation of PHAse Diagrams (CALPHAD) technique

[49,50]. It therefore appears that flat microstructural facets, which indicate the limitations of crack growth paths, appear in greater numbers on the fatigue fracture surface of CoCrFeNiTiMo than on Alloy 718, as shown in Figs. 13 and 14. According to our previous study, the flat facets on the fatigue fracture surface were on the {111} slip plane [51]. Planar cracks in CoCrFeNiTiMo alloy propagating along the slip band were in fact observed, as shown in Figure 18. In addition, the few deformations around the fatigue crack in the CoCrFeNiTiMo alloy shown in Fig. 17 indicate that the fatigue crack propagated along a limited slip plane. Koyama et al. pointed out that high slip planarity tends to direct the fatigue crack growth path to the slip plane [22]. Furthermore, cyclic slip morphology shown in Fig. 15 also supported the slip planarity of CoCrFeNiTiMo alloy. Hence, it appears that the fatigue crack of CoCrFeNiTiMo alloy propagated with more planar slip deformation than that of Alloy 718.

Several reports deal with the effect of slip planarity on fatigue property. Murayama et al. demonstrated that the ΔK_{th} of long fatigue cracks increases as SFE decreases due to the effects of slip planarity on adding Mo and N to austenitic stainless steel [52]. Seifi et al. reported on the excellent ΔK_{th} of HEA and its flat microstructural facets on fatigue fracture surfaces [17]. Vasudevan et al. also pointed out, after evaluating a mass of published FCG data, that the FCG resistance of planar slip material is usually higher than that of homogeneous slip material [48].

Zhang et al. examined the effect of Cr content on the fatigue strength of smooth Ni-Cr alloy specimens, focusing on changes in SFE [53]. According to their experimental study, the fatigue strength / tensile strength ratio remained constant even though the SFE and fatigue strength varied as a function of Cr content. Further, Koyama et al. investigated fatigue behaviour of stainless steel and HEA [22] which exhibit planar slip,

but their fatigue strengths were able to be normalized with tensile strength. Li et al. also reported that the fatigue strength ratio, and fatigue strength / tensile strength in more than ten published data sets on HEA were mainly distributed around 0.33 - 0.36 provided that ultrafine grained material was excluded [13]. This fatigue strength ratio of HEA is at a normal level compared to conventional steels, unlike long crack growth resistance.

Based on the above previous reports, it is possible to state that higher slip planarity increases long crack growth resistance but does not contribute to SFC growth resistance, which is related to fatigue strength, in smooth specimens. The gap between short and long fatigue crack growth behaviour seen in our experimental results would therefore be expected.

One possible explanation that would illuminate the effects of slip planarity on short and long fatigue crack growth properties is slip constraint due to adjoint grains. Figure 19 shows the schematics of the growth path of two typical cracks across a grain boundary. This figure assumes crack growth along slip planes. The twisted angle θ and ψ of two adjoint slip planes is important in directing the crack path if it crosses the grain boundary. From the perspective of slip transfer, Jimenez et al. demonstrated, based on three-dimensional analysis, that the slip plane which minimizes θ and ψ was the most likely fatigue crack path [54]. This crack growth resistance is schematically described in Figure 19. When the twisted angle of θ is small, cracks readily move on to the adjoint slip plane of the next grain, as shown in Fig. 19 a). In contrast, if the two slip planes are twisted, as in Fig. 19 b), the crack is likely to grow along a complex path to fill the geometrical gap that results from the angle θ. As a result, the FCG resistance of the growth path shown in Fig. 19 b) should greater than that of Fig. 19 a).

Short fatigue cracks are therefore considered to have a higher probability of realizing the state shown in Fig. 19 a) because a crack initiated in the weakest part of the specimen should grow preferentially. If several short fatigue cracks initiate in the specimen, the crack should grow faster if the state in Fig. 19 a) has been realized. In contrast, a long crack will potentially have a larger area that is in the state shown in Fig. 19 b) because the crack tip includes a larger number of grains than does a short crack. We conclude that planar slip in CoCrFeNiTiMo alloy increases the FCG resistance of the state shown in Fig. 19 b) only, because when a cross slip is suppressed due to planar slip of CoCrFeNiTiMo alloy, it makes it more difficult to fill the angle gap shown in Fig. 19 b). In contrast, it appears relatively easy to fill the gap in Alloy 718 due to its high SFE which possibly facilitates cross slip. On the other hand, the effect of slip planarity on FCG resistance in the state in Fig. 19 a) appears to be small. In fact, the SFCG rate of CoCrFeNiTiMo and Alloy 718 was comparable. Slow FCG of sub cracks were observed in CoCrFeNiTiMo alloy probably because the crack tip, by chance, reaches the state in Fig. 19 b) as the crack grows. These explanations are summarized in Table 4. This is a new and unique concept that explains the effect of slip planarity on fatigue property.

We believe that the explanation above is the reason why long fatigue cracks in CoCrFeNiTiMo alloy exhibited excellent FCG resistance while short FCG resistance was at the normal level from the perspective of slip planarity. Taking into consideration the recent rapid improvements in HEAs, the effect of slip planarity on fatigue property has become increasingly important. This study successfully demonstrates and explains the unique fatigue feature of CoCrFeNiTiMo and the effect of slip planarity by using systematic fatigue data obtained for the first time. Short and long FCG data from the

perspective of slip planarity, the first ever to be obtained, was necessary to elucidate the complex effects of planar slip. More detailed observation of slip deformation, such as slip planarity or dislocation morphology, related to FCG will be found in the next issue.

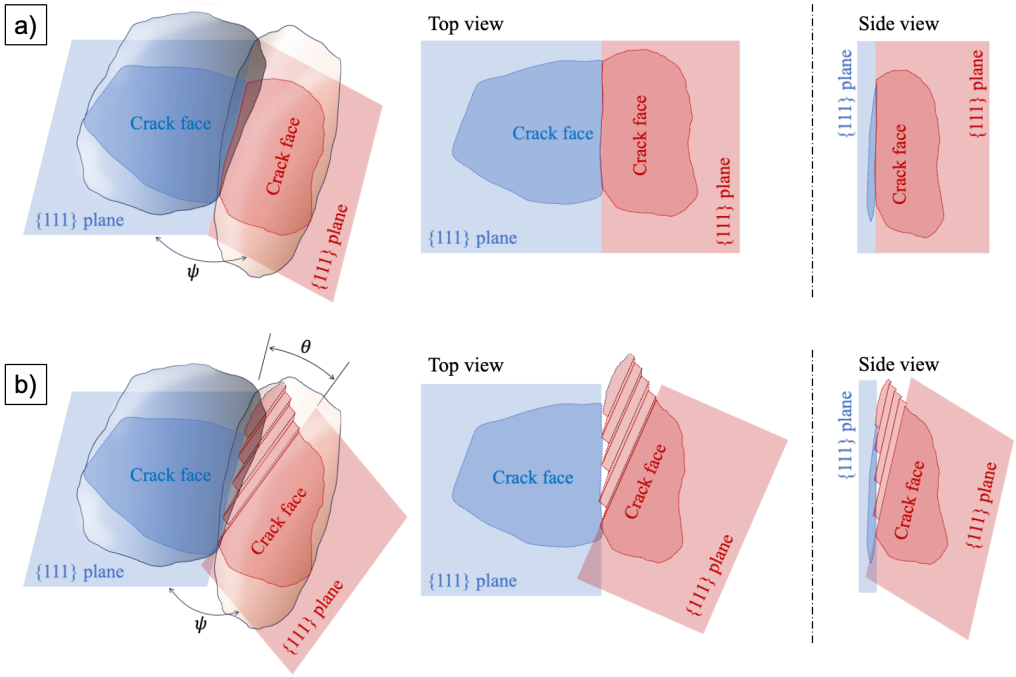

Figure 19. Schematics of two typical crack growth paths across a grain boundary for a) continuous slip plane and b) twisted slip plane. Short and long fatigue cracks potentially close to the state of a) and b) respectively.

Table 4. Summary of the possible relationship of crack character in Fig. 19, short / long FCG regime and the effect of slip planarity

	Continuous slip plane, Fig. 19 a)	Twisted slip plane, Fig. 19 b)
Potential to appear	Potentially appears in a **short crack regime** in relation to the weakest-link theory.	Will always appear in a **long crack regime** which has numerous grains at the crack front.
Effect of slip planarity	Possibly negligible or enhances FCG as the slip concentration.	**Planar slip possibly inhibits FCG** due to the constraint of cross slip when filling the gap of θ.

6. Conclusions

In this study, the fatigue characteristics of additively-formed MPEAs of CoCrFeNiTiMo were systematically compared with conventional hot-rolled and additively-formed Alloy 718 nickel-based super alloys which have similar mechanical properties. The following conclusions can be drawn.

1. The fatigue strength of CoCrFeNiTiMo alloy was comparable to that of Alloy 718 in smooth specimens, whereas that of the notched specimen was 50 % higher.
2. Regardless of load ratio, CoCrFeNiTiMo exhibited superior FCG resistance that greatly surpassed that of conventional Fe and Ni alloys. In contrast, the short FCG resistance of CoCrFeNiTiMo was comparable to that of Alloy 718.
3. Investigation of fatigue fracture surfaces and microscopic cross-sectional fatigue cracks indicates that CoCrFeNiTiMo alloy exhibits more planar slip deformation than Alloy 718.
4. The excellent notch fatigue strength of CoCrFeNiTiMo alloy quantitatively corresponds to the ΔK_{th} value for long crack data. In addition, CoCrFeNiTiMo alloy has the highest level of FCG resistance ever officially published.
5. The gap between short and long FCG resistance of Alloy 718 and CoCrFeNiTiMo alloy was successfully explained in terms of the slip constraint stimulated by slip planarity when fatigue cracks extend across grain boundaries.

Acknowledgments

We would like to thank Ms. Nana Tottori for assistance with the SEM / EBSD observations and short fatigue crack measurements.

Data availability

Due to technical or time limitations, the raw/processed data employed to reproduce these findings cannot be shared at this time.

References

[1] B. Cantor, I.T.H. Chang, P. Knight, A.J.B. Vincent, Microstructural development in equiatomic multicomponent alloys, Mater. Sci. Eng. A. 375–377 (2004) 213–218. doi:10.1016/j.msea.2003.10.257.

[2] J.W. Yeh, S.K. Chen, S.J. Lin, J.Y. Gan, T.S. Chin, T.T. Shun, C.H. Tsau, S.Y. Chang, Nanostructured high-entropy alloys with multiple principal elements: Novel alloy design concepts and outcomes, Adv. Eng. Mater. 6 (2004) 299–303. doi:10.1002/adem.200300567.

[3] O.N. Senkov, J.D. Miller, D.B. Miracle, C. Woodward, CALPHAD : Computer Coupling of Phase Diagrams and Thermochemistry Accelerated exploration of multi-principal element alloys for structural applications, Calphad. 50 (2015) 32–48. doi:10.1016/j.calphad.2015.04.009.

[4] Z. Li, K.G. Pradeep, Y. Deng, D. Raabe, C.C. Tasan, Metastable high-entropy dual-phase alloys overcome the strength-ductility trade-off, Nature. 534 (2016) 227–230. doi:10.1038/nature17981.

[5] B. Gludovatz, A. Hohenwarter, D. Catoor, E.H. Chang, E.P. George, R.O. Ritchie, A fracture-resistant high-entropy alloy for cryogenic applications, Science (80-.). 345 (2014) 1153–1158. doi:10.1126/science.1254581.

[6] T. Fujieda, H. Shiratori, K. Kuwabara, M. Hirota, T. Kato, K. Yamanaka, Y. Koizumi, A. Chiba, S. Watanabe, CoCrFeNiTi-based high-entropy alloy with superior tensile strength and corrosion resistance achieved by a combination of additive manufacturing using selective electron beam melting and solution treatment, Mater. Lett. 189 (2017) 148–151. doi:10.1016/j.matlet.2016.11.026.

[7] T. Fujieda, M. Chen, H. Shiratori, K. Kuwabara, K. Yamanaka, Y. Koizumi, A. Chiba, S. Watanabe, Mechanical and corrosion properties of CoCrFeNiTi-based high-entropy alloy additive manufactured using selective laser melting, Addit. Manuf. 25 (2019) 412–420. doi:https://doi.org/10.1016/j.addma.2018.10.023.

[8] K. Kwak, Y. Okamura, Y. Mine, K. Takashima, S. Koseki, S. Ando, K. Kuwabara, Micro-mechanical characterisation of slip behaviour and precipitation strengthening in CoCrFeNiTiMo alloy additively manufactured by laser powder bed fusion, Mater. Sci. Eng. A. 840 (2022) 142970. doi:10.1016/j.msea.2022.142970.

[9] K. Kuwabara, T. Kimura, H. Shiratori, Y. Daigo, Enhanced strengthening effect of aging heat treatment found in additively-formed CoCrFeNiTi-based multiprincipal element alloy, Mater. Today Commun. 35 (2023) 105938. doi:https://doi.org/10.1016/j.mtcomm.2023.105938.

[10] Y.L. Chou, J.W. Yeh, H.C. Shih, The effect of molybdenum on the corrosion behaviour of the high-entropy alloys Co 1 . 5 CrFeNi 1 . 5 Ti 0 . 5 Mo x in aqueous environments, Corros. Sci. 52 (2010) 2571–2581. doi:10.1016/j.corsci.2010.04.004.

[11] Y.L. Chou, J.-W. Yeh, H.C. Shih, Effect of Molybdenum on the Pitting Resistance of Co 1.5 CrFeNi 1.5 Ti 0.5 Mo x Alloys in Chloride Solutions, Corrosion. 67 (2011) 85001–85002. doi:10.5006/1.3613646.

[12] J. Rackwitz, Q. Yu, Y. Yang, G. Laplanche, E.P. George, A.M. Minor, R.O. Ritchie, Effects of cryogenic temperature and grain size on fatigue-crack propagation in the medium-entropy CrCoNi alloy, Acta Mater. 200 (2020) 351–365. doi:10.1016/j.actamat.2020.09.021.

[13] W. Li, S. Chen, P.K. Liaw, Discovery and design of fatigue-resistant high-entropy alloys, Scr. Mater. 187 (2020) 68–75. doi:10.1016/j.scriptamat.2020.05.047.

[14] Y. Furuya, H. Nishikawa, H. Hirukawa, N. Nagashima, E. Takeuchi, Catalogue of NIMS fatigue data sheets, Sci. Technol. Adv. Mater. 20 (2019) 1055–1072. doi:10.1080/14686996.2019.1680574.

[15] Y. Furuya, H. Nishikawa, H. Hirukawa, N. Nagashima, E. Takeuchi, Fatigue properties of titanium alloys disclosed in NIMS fatigue data sheets, Sci. Technol. Adv. Mater. Methods. (2023) 2285711. doi:10.1080/27660400.2023.2285711.

[16] Y. Furuya, H. Nishikawa, H. Hirukawa, N. Nagashima, E. Takeuchi, NIMS fatigue data sheet on low- and high-cycle fatigue properties of A2017-T4 (Al-4.0Cu-0.6Mg) aluminium alloy, Sci. Technol. Adv. Mater. Methods. 3 (2023) 0–10. doi:10.1080/27660400.2023.2234272.

[17] M. Seifi, D. Li, Z. Yong, P.K. Liaw, J.J. Lewandowski, Fracture Toughness and Fatigue Crack Growth Behavior of As-Cast High-Entropy Alloys, Jom. 67 (2015) 2288–2295. doi:10.1007/s11837-015-1563-9.

[18] X.H. An, S.D. Wu, Z.G. Wang, Z.F. Zhang, Significance of stacking fault energy in bulk nanostructured materials: Insights from Cu and its binary alloys as model systems, Prog. Mater. Sci. 101 (2019) 1–45. doi:10.1016/j.pmatsci.2018.11.001.

[19] C. Wagner, G. Laplanche, Effects of stacking fault energy and temperature on grain boundary strengthening, intrinsic lattice strength and deformation mechanisms in CrMnFeCoNi high-entropy alloys with different Cr/Ni ratios, Acta Mater. 244 (2023) 118541. doi:10.1016/j.actamat.2022.118541.

[20] K. Katagiri, A. Omura, K. Koyanagi, J. Awatani, T. Shiraishi, H. Kaneshiro, Early stage crack tip dislocation morphology in fatigued copper, Metall. Trans. A. 8 (1977) 1769–1773. doi:10.1007/BF02646881.

[21] P. Neumann, New experiments concerning the slip processes at propagating fatigue cracks-I, Acta Metall. 22 (1974) 1155–1165. doi:10.1016/0001-6160(74)90071-6.

[22] K. Suzuki, M. Koyama, S. Hamada, K. Tsuzaki, H. Noguchi, Planar slip-driven fatigue crack initiation and propagation in an equiatomic CrMnFeCoNi high-entropy alloy, Int. J. Fatigue. 133 (2020) 105418. doi:10.1016/j.ijfatigue.2019.105418.

[23] J. A.J.McEVILY, R.C. BOETTNER, on Fatigue Crack Propagation in F.C.C. Metals, Acta Metall. 11 (1963) 725–743.

[24] C. Bathias, R.M. Pelloux, Fatigue crack propagation in martensitic and austenitic steels, Metall. Trans. 4 (1973) 1265–1273. doi:10.1007/BF02644521.

[25] R.O. Ritchie, J. Lankford, Small fatigue cracks: A statement of the problem and potential solutions, Mater. Sci. Eng. 84 (1986) 11–16. doi:10.1016/0025-5416(86)90217-X.

[26] Y. Yuan, Y. Gu, C. Cui, T. Osada, Z. Zhong, T. Tetsui, T. Yokokawa, H. Harada, Influence of Co content on stacking fault energy in Ni-Co base disk superalloys, J. Mater. Res. 26 (2011) 2833–2837. doi:10.1557/jmr.2011.346.

[27] H. Nishikawa, Y. Furuya, H. Kitano, T. Nakamura, K. Kuwabara, Y. Kanegae, D. Kang, K. Aota, In-situ observation of microstructurally small fatigue crack initiation and growth behaviors of additively-manufactured alloy 718, Mater. Sci. Eng. A. 835 (2022) 142682. doi:10.1016/j.msea.2022.142682.

[28] K. Habib, H. Nishikawa, Y. Furuya, S. Emura, The Role of Crystallographic Texture and Basal Plane Slip on Microstructurally Short Fatigue Crack Initiation and Propagation in Forged Billet and Rolled Bar Ti-6Al-4V Alloy, Metall. Mater. Trans. A. 52 (2021) 3821–3838. doi:10.1007/s11661-021-06344-z.

[29] R.W. Landgraf, J. Morrow, T. Endo, Determination of the Cyclic Stress-Strain Curve, J. Mater. JMLSA. 4 (1969) 176–188.

[30] H. Nishikawa, Y. Furuya, Cyclic Yield Characterization for Low-Carbon Steel with HAZ Microstructures, Mater. Trans. 60 (2019).

[31] ASTM E647 Standard Test Method for Measurement of Fatigue Crack Growth Rates, ASTM International, West Conshohocken, PA, 2023.

[32] H. Nishikawa, Y. Furuya, Development of a Method for Evaluating Microstructurally Small Fatigue Crack Initiation and Growth by Using an Automatic System for *In Situ* Observation in Conjunction with a Digital-Image Correlation Technique, ISIJ Int. 60 (2020) 2090–2096. doi:10.2355/isijinternational.ISIJINT-2019-823.

[33] T. Masumura, Y. Seto, T. Tsuchiyama, K. Kimura, Work-hardening mechanism in high-nitrogen austenitic stainless steel, Mater. Trans. 61 (2020) 678–684. doi:10.2320/matertrans.H-M2020804.

[34] P.K. Liaw, T.R. Lea, W.A. Logsdon, Near-threshold fatigue crack growth behavior in metals, Acta Metall. 31 (1983) 1581–1587. doi:10.1016/0001-6160(83)90155-4.

[35] A.K. Vasudévan, K. Sadananda, N. Louat, Two critical stress intensities for threshold fatigue crack propagation, Scr. Metall. Mater. 28 (1993) 65–70. doi:10.1016/0956-716X(93)90538-4.

[36] A.K. Vasudeven, K. Sadananda, N. Louat, A review of crack closure, fatigue crack threshold and related phenomena, Mater. Sci. Eng. A. 188 (1994) 1–22. doi:10.1016/0921-5093(94)90351-4.

[37] K. Vasudi, Classification of Fatigue Crack Growth Behavior K sustain Cs ~ L ~ ----4-1ed / -i max, (1995) 1221–1234.

[38] W. ELBER, FATIGUE CRACK CLOSURE UNDER CYCLIC TENSION, Eng. Fract. Mech. 2 (1970) 37–45. doi:10.1016/0013-7944(70)90028-7.

[39] E. Wolf, Fatigue crack closure under cyclic tension, Eng. Fract. Mech. 2 (1970) 37–45. doi:https://doi.org/10.1016/0013-7944(70)90028-7.

[40] R. Kakimoto, M. Koyama, K. Tsuzaki, EBSD- And ECCI-based Assessments of Inhomogeneous Plastic Strain Evolution Coupled with Digital Image Correlation, ISIJ Int. 59 (2019) 2334–2342. doi:10.2355/isijinternational.ISIJINT-2019-232.

[41] A. Heinz, P. Neumann, Crack initiation during high cycle fatigue of an austenitic steel, Acta Metall. Mater. 38 (1990) 1933–1940. doi:10.1016/0956-7151(90)90305-Z.

[42] L. Llanes, C. Laird, The role of annealing twin boundaries in the cyclic deformation of f.c.c. materials, Mater. Sci. Eng. A. 157 (1992) 21–27. doi:https://doi.org/10.1016/0921-5093(92)90094-H.

[43] R.E. PETERSON, Notch sensitivity, Met. Fatigue. (1959) 293–306. https://cir.nii.ac.jp/crid/1573668924078557952.

[44] K. Tanaka, Engineering formulae for fatigue strength reduction due to crack-like notches, Int. J. Fract. 22 (1983) 39–46. doi:10.1007/BF00942722.

[45] M.H. El Haddad, T.H. Topper, K.N. Smith, Prediction of non propagating cracks, Eng. Fract. Mech. 11 (1979) 573–584. doi:https://doi.org/10.1016/0013-7944(79)90081-X.

[46] K. Minakawa, Y. Matsuo, A.J. McEVILY, The influence of a duplex microstructure in steels on fatigue crack growth in the near-threshold region, Metall. Trans. A. 13 (1982) 439–445. doi:10.1007/BF02643352.

[47] K. Tanaka, C. Masuda, S. Nishijima, the Generalized Relationship Between the Parameters, 15 (1981) 259–264.

[48] A.K. Vasudevan, K. Sadananda, K. Rajan, Role of microstructures on the growth of long fatigue cracks threshold fatigue crack growth; two threshold parameters K * max and K * th ; microstructure-grain size and precipitate spacing; slip mode; crack deflection; stacking fault; pure iron; steel all, Int. J. Fatigue. 19 (1997) 151–159.

[49] A.P. Miodownik, W. Genminy, The Calculation of Stacking Fault in FE-Ni-CR Alloys, Calphad. 2 (1978) 207–226.

[50] A.P. Miodownik, X. Li, N. Saunders, J.-P. Schille, Modelling of Creep in Nickel Based Superalloys, 6 Th Int. Charles Parsons Turbine Conf. (2003).

[51] H. Nishikawa, Y. Furuya, T. Osada, K. Kawagishi, T. Hara, Three-dimensional high-resolution crystallographic observation of the entire volume of microstructurally small fatigue cracks in Ni-Co based superalloy, Scr. Mater. 222 (2023) 115026. doi:10.1016/j.scriptamat.2022.115026.

[52] M. Murayama, K. Hono, H. Hirukawa, T. Ohmura, S. Matsuoka, Combined effect of molybdenum and nitrogen on the fatigued microstructure of 316 type

austenitic stainless steel, Scr. Mater. 41 (1999) 467–473. doi:10.1016/S1359-6462(99)00194-3.

[53] Y.J. Zhang, D. Han, X.W. Li, Improving the stress-controlled fatigue life of low solid-solution hardening Ni-Cr alloys by enhancing short range ordering degree, Int. J. Fatigue. 149 (2021). doi:10.1016/j.ijfatigue.2021.106266.

[54] M. Jiménez, W. Ludwig, D. Gonzalez, J.M. Molina-Aldareguia, The role of slip transfer at grain boundaries in the propagation of microstructurally short fatigue cracks in Ni-based superalloys, Scr. Mater. 162 (2019) 261–265. doi:10.1016/j.scriptamat.2018.11.008.